Level lifetimes in ^{32}P obtained using the Doppler-shift attenuation method with thick molecular targets

R. Bhattacharjee, S. S. Bhattacharjee, K. Basu, P. V. Rajesh, R. Raut, S. S. Ghugre, D. Das, A. K. Sinha, L. Chaturvedi, U. Garg, S. Ray, B. K. Yogi, M. Kumar Raju, R. Chakrabarti, S. Mukhopadhyay, A. Dhal, R. P. Singh, N. Madhavan, and S. Muralithar

Phys. Rev. C **90**, 044319 — Published 22 October 2014

DOI: 10.1103/PhysRevC.90.044319

Level lifetimes in ^{32}P obtained using the Doppler-shift attenuation method with thick molecular targets

R. Bhattacharjee, S. S. Bhattacharjee, K. Basu, P. V. Rajesh, R. Raut,* S. S. Ghugre, D. Das, and A. K. Sinha
UGC-DAE Consortium for Scientific Research, Kolkata Centre, Kolkata 700098, India

L. Chaturvedi
Guru Ghasidas University, Bilaspur 495009, India

U. Garg
Department of Physics, University of Notre Dame, Notre Dame, Indiana 46556, USA

S. Ray
Amity Institute of Nuclear Science and Technology, Amity University, Noida, Uttar Pradesh 201303, India

B. K. Yogi
Department of Physics, Government College, Kota 324009, India

M. Kumar Raju
Nuclear Physics Department, Andhra University, Visakhapatnam 530003, India

R. Chakrabarti and S. Mukhopadhyay
Nuclear Physics Division, Bhabha Atomic Research Centre, Mumbai 400085, India

A. Dhal, R. P. Singh, N. Madhavan, and S. Muralithar
Inter University Accelerator Centre, Aruna Asaf Ali Marg, New Delhi 110067, India

(Dated: October 7, 2014)

Level lifetimes in the ^{32}P nucleus have been determined using the Doppler Shift Attenuation Method (DSAM). Conventional DSAM measurements employ a thin target on a thick, high Z backing. An extension of the technique to thick molecular targets is presented. The necessary modifications in the standard analysis procedures, pertaining to the incorporation of stopping power estimations for molecular media and evolution of residue cross-section in thick target, have been implemented. Further, x-ray powder diffraction (XRD) and scanning electron-microscopy (SEM) have also been carried out to probe the structural composition of the target. The lifetime results have been validated with respect to the previous measurements and upper limit on lifetimes of seven levels have been determined for the first time. Large basis shell model calculations have been carried out and compared with the experimental measurements.

PACS numbers: 23.20.Lv,21.10.Hw,21.60.Cs

I. INTRODUCTION

The high-spin states in nuclei in the vicinity of the island of inversion (interface of the *sd-fp* orbitals), eg. ^{26}Mg, ^{33}S, ^{32,33,34}P, have been the subjects of extensive experimental and theoretical investigations [1–6] in recent times. The low lying positive parity states in these nuclei are expected to be dominated by pure *sd* configurations while the negative parity states involve excitations to the fp shell. Thus, the energy systematics of negative parity levels can be indicative of the evolution of the *sd-fp* shell gap in the region. The level structure of some of these $sdpf$ nuclei are well established experimentally providing a testing ground for the large basis spherical shell model calculations [2, 7]. We have previously reported our spectroscopic investigation of the ^{26}Mg, ^{32,33,34}P, ^{33}S [3, 5, 6], using heavy-ion induced fusion-evaporation reactions, wherein the level structures have been extended to higher spin domain. However, an unambiguous understanding of the structure requires information on the excited level lifetimes that helps us to identify the underlying microscopic configurations of the states. Herein we report the lifetime measurements for levels of the ^{32}P nucleus, using DSAM with thick molecular target setup, along with a comparison with the shell model investigations.

*Electronic address: rraut@alpha.iuc.res.in

The lifetimes of levels in ^{32}P, below an excitation

energy of 6.4 MeV, have been reported by Kangasmäki *et al.* [8] with due reference and comparison to the previous measurements (Table II of Ref.[8]). In the context of the present work, the lifetimes of the 1323 keV, 1755 keV, 3149 keV, 3444 keV and 4276 keV are of importance. Of these states, only the lifetimes of the 1323 keV and the 1755 keV levels have been measured by Kangasmäki *et al.* while for the other three states, the lifetimes have been reanalyzed with respect to the previous measurements using the Monte Carlo approach. The 3149 keV state had previously been measured by Carr *et al.* [9] and Eijkern *et al.* [10] and the results from these measurements are in good agreement. The re-evaluation of the 3149 keV level lifetime by Kangasmäki *et al.* complies with these reported values. The lifetime of the 3444 keV state had only been measured by Carr *et al.* [9] and the re-analysis by Kangasmäki *et al.* is in agreement with the measured value. The 3444 keV level with spin-parity $J^{\pi} = 4^{-}$ is of particular importance since this is the lowest negative parity level and represents excitation to the pf shell in the ^{32}P nucleus, wherefrom an indication of the *sd-fp* shell gap in the region can be obtained. The lifetime of the 4276 keV level had only been measured by Eijkern *et al.* [10] and the re-analysis by Kangasmäki *et al.* is in agreement, within the uncertainties, with the reported value. It is noteworthy to point out that the aforesaid measurements of the lifetimes in the ^{32}P nucleus have been carried out using modest experimental setups and may warrant a re-examination of these results in the light of contemporary facilities. In addition, our earlier reported spectroscopic investigation of the ^{32}P nucleus [5] led to the observation of new levels, populated through heavy-ion induced fusion-evaporation reaction. Lifetime measurements for these levels are in requirement to probe the underlying microscopic structure.

A wide range of experimental techniques are applied depending on the order of lifetime being measured. The Doppler Shift Attenuation Method (DSAM) is one of the commonly used technique to measure lifetimes in the range of few tens of femtoseconds (10^{-15} s) to few picoseconds (10^{-12} s). The method is based on the observed Doppler effects as the recoiling nuclei, produced in a nuclear reaction, slow down (and eventually stop) within the target and / or the backing medium (stopping medium) while de-exciting with the emission of γ-ray transitions. The Doppler effect consequently introduces either a shift or a broadening in the observed γ-ray energy, depending on both the level lifetime as well as the stopping time. The analysis of this observed shape / shift, with due incorporation of the slowing down of the recoils in the stopping medium and the time evolution of the level of interest (the formation time and it's subsequent decay), facilitates the extraction of the level lifetimes. These measurements are performed at relatively large recoil velocities, ($\beta \geq 2\%$), which results in a longer stopping time of the recoiling nuclei and makes the method sensitive to lifetimes typically in the aforementioned range.

Conventionally, the Doppler Shift Attenuation Method (DSAM) is carried out using thin target, on a high Z *elemental* backing material . The choice of thin target ensures that the energy loss of the recoiling nuclei occurs predominantly in a single medium *i.e* the backing medium. Further, the backing medium is chosen to be of elemental nature, reducing the uncertainties on the stopping simulations which, from the available experimental data, are better known for commonly used backing media like gold, tantalum, lead etc. The Doppler Broadened γ-ray lineshapes are analyzed, for example, using the program LINESHAPE [11]. However, the code is primarily appropriate for the DSAM experiments carried out using thin target along with a thick elemental backing and hence, would require modifications to incorporate the alternative experimental scenarios as discussed herein.

The spectroscopic investigations of certain nuclei may require the use of a target which cannot be easily prepared in it's pure elemental form. For example, the use of a neutron rich target (^{18}O) as well as a neutron rich projectile (^{18}O), could result in the population of high-spin states in nuclei at the interface of the *sd-fp* orbitals. It is noteworthy to mention that the ^{18}O target can only be fabricated in a molecular form such as Vanadium (V_2O_5) or Tantalum (Ta_2O_5) Pentoxide. Our group has reported the use of thick Ta_2O_5 target, enriched in ^{18}O, in the spectroscopic studies of these nuclei [3, 5, 6]. The Doppler lineshapes observed for the γ-ray transitions in these experiments cannot be analyzed within the purview of the standard LINESHAPE package. The present paper reports the modifications required to analyze the Doppler shapes obtained from thick molecular targets acting also as the stopping medium, validates the modifications with respect to the previously measured lifetimes in the ^{32}P nucleus, extends the analysis to determine hitherto unknown lifetimes and compares the results with the shell model calculations.

II. EXPERIMENTAL DETAILS

The high spin states in ^{32}P, have been populated using the ^{18}O(^{16}O, np)^{32}P reaction at an incident beam energy of 34 MeV. The details of the experimental setup are outlined in Ref. [3]. The neutron-rich ^{18}O, has been prepared by heating the Ta foil of thickness $\sim 50\ mg/cm^2$, in an enriched ^{18}O atmosphere, resulting in the formation on Ta_2O_5 on either side of the foil. The thickness of the Ta_2O_5 on either side of the foil has been estimated to be 9.25 mg/cm^2. The de-exciting

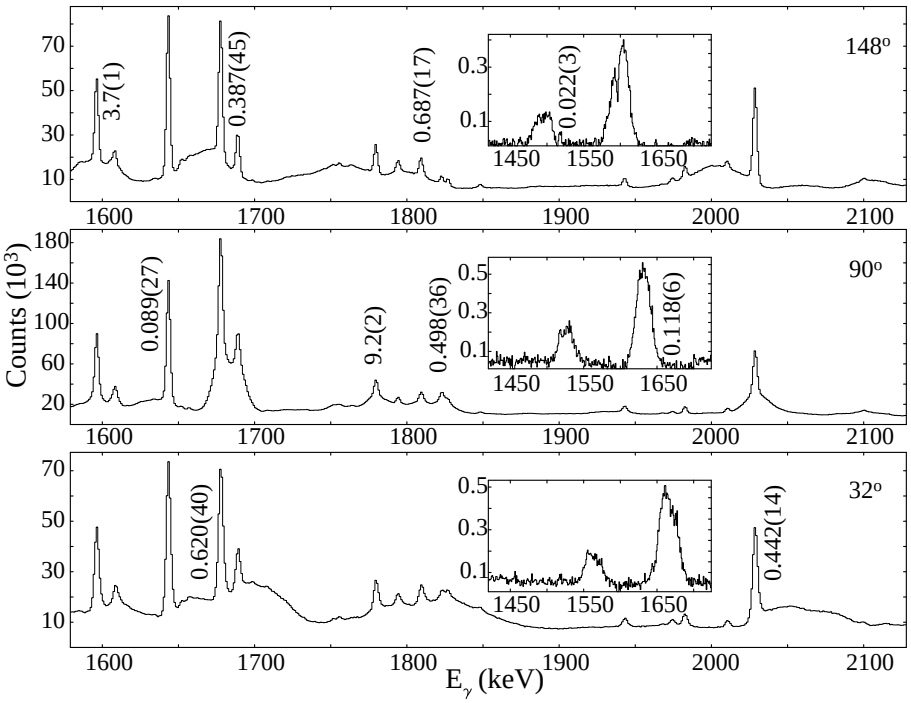

FIG. 1: Angle dependent projection spectra exhibiting Doppler effects on the γ-ray peaks observed in the present work. The labels indicate the reported lifetimes in ps [12]. The inset illustrates the Doppler shifted 1526 keV and 1631 keV (from ^{29}Si) peaks at forward and backward angles from very short lived levels.

γ-rays have been detected using the Indian National Gamma Array (INGA) [13], stationed at the 15 UD Pelletron Accelerator Centre at IUAC, New Delhi. The Clover detectors of the INGA setup were placed at $\theta = 32\,^{\circ}, 57\,^{\circ}, 90\,^{\circ}, 123\,^{\circ}, 148\,^{\circ}$, with respect to the beam-axis. The energy calibration has been carried out using the radioactive sources as well as the beam-off radioactivity data, which provided us with high energy calibration points. The data has been sorted in the angle dependent $E_\gamma - E_\gamma$ matrices with the 90° detectors on one axis and the detectors at one of the remaining angles on the other axis. The spectra demonstrating the Doppler effects (shapes) on the observed γ-rays from the residual nuclei at forward and backward angles, with gates applied on coincident transitions at 90°, are illustrated in Fig. 1. The matrices were formed with energy dispersion of 0.5, 1 & 2 keV/channel, which have been analyzed to ensure consistency of the extracted lifetimes. The observed γ-ray at the five available angles have been analyzed simultaneously (as detailed in the subsequent sections) for determination of the level-lifetimes.

III. PROGRAMMING MODIFICATIONS FOR DATA ANALYSIS

We report here the modifications in the LINESHAPE program [11] for the determination of the lifetimes of nuclear levels populated using a thick molecular target. LINESHAPE program essentially comprises of three major sub-programs, as detailed below.

1. DECHIST. It simulates the velocity (β) evolution of a given number of recoiling nuclei in the target and the backing media, using Monte Carlo techniques. It uses a set of stopping powers for the beam and the recoiling nuclei in the target and the backing media, that are computed using either (i) Ward's effective charge [14] and Ziegler's proton stopping powers [15] or (ii) Ziegler's heavy-ion stopping powers [15] or (iii) Shell-corrected Northcliffe and Schilling stopping powers [16]

2. HISTAVER. It converts the time-dependent velocity histories of the recoiling nuclei into velocity profiles as viewed by the detectors at various angles.

3. LINESHAPE. It calculates the shapes for the γ-ray transitions of interest, at different angles and performs a least-square fit of the experimentally observed shapes to determine the level lifetimes. The level-lifetime (τ), side-feeding times (τ_{sf}) and

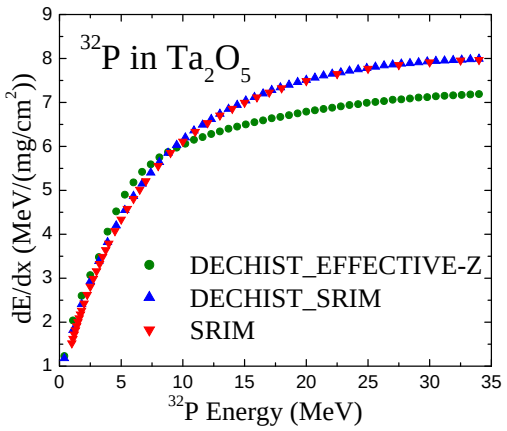

FIG. 2: (Color online) Stopping powers of ^{32}P ions in Ta_2O_5 using SRIM (labelled as SRIM in the legend), DECHIST with SRIM input and interpolation (DECHIST_SRIM) and DECHIST with effective Z and effective A for the Ta_2O_5 target (DECHIST_EFFECTIVE-Z).

the spectrum parameters (such as centroid, background) are the parameters for the least-square fitting procedure.

The modifications in the LINESHAPE package have been carried out in the calculation of the stopping powers and incorporation of the cross-section dependence on the beam energy in the DECHIST program. These modifications are detailed herein.

A. Stopping Powers

The default prescription for computing the stopping power in the DECHIST program considers elemental medium only. A possible solution to include a compound medium would require using an *effective Z* and an *effective A* to approximate the molecular media to an equivalent elemental form. The expressions used to calculate these quantities are as follows.

$$A_{eff} = \Sigma_i w_i A_i \tag{1}$$

$$Z_{eff} = A_{eff} \Sigma_i \frac{Z_i w_i}{A_i} \tag{2}$$

where w_i, A_i and Z_i are respectively the weight / mass fraction of the species (element) i, its mass number and its atomic number. Fig. 2 illustrates the DECHIST calculated stopping power (labelled as DECHIST_EFFECTIVE-Z) of Ta_2O_5 medium for ^{32}P ions, using $Z_{eff} = 61$ and $A_{eff} = 148$.

Updated stopping powers, for heavy ions in elemental as well as molecular media are available in contemporary software like SRIM [17], which have been exhaustively benchmarked with respect to the experimental data and are considered to be more reliable. It would thus be appropriate to incorporate these stopping powers in the lifetime analysis. The stopping powers of ^{32}P ions in Ta_2O_5 from SRIM are included in Fig. 2. As is evident from the figure, the two approaches are approximately in agreement at lower energies, but deviate considerably in the higher energy domain, of kinematic relevance in the typical stopping calculations.

In the light of the reliability of the SRIM stopping powers, these have been incorporated in the modified DECHIST program and used in the current work. The DECHIST program calculates the stopping powers at 61 hard-coded energies, ranging from 1 keV to 1000 MeV, for the residue in the target and the backing, as well as for the beam in the target. The stopping power required for all the intermediate energies are calculated through an in-built interpolation subroutine. The modified version of the program requires the user to provide these stopping powers, as calculated from SRIM (operating in batch mode), at these 61 energies through an input file. As already mentioned above, the DECHIST calculates the stopping powers at relevant energies through interpolation. The interpolated stopping powers for ^{32}P + Ta_2O_5 case, as calculated by the modified DECHIST program, are also presented in the Fig. 2 (DECHIST_SRIM). The overlap between the stopping powers calculated by SRIM and those calculated by DECHIST, with SRIM inputs and appropriate interpolation, validates the modification. A similar attempt to incorporate the SRIM calculated stopping powers in the LINESHAPE package has also been undertaken by Snyder *et al.* [18], though for an elemental medium.

B. Cross-section Dependence

A thin target ensures that the production cross section for the recoils, as a function of the beam energy, across the target can be assumed to be constant. Use of a thick target results in a substantial change (decrease) in the energy of the incident projectile as it traverses the target thickness and thus affect the production cross section of the residues along the depth of the target. Further, in a thick target, one needs to determine the thickness of the target that actually contributes to the residue production while the rest of the target thickness acts only as the stopping medium. The knowledge of target thickness contributing to the residue production follows from the information on the cross section dependence on the beam energy and the evolution of the latter along the target thickness. The original version of the

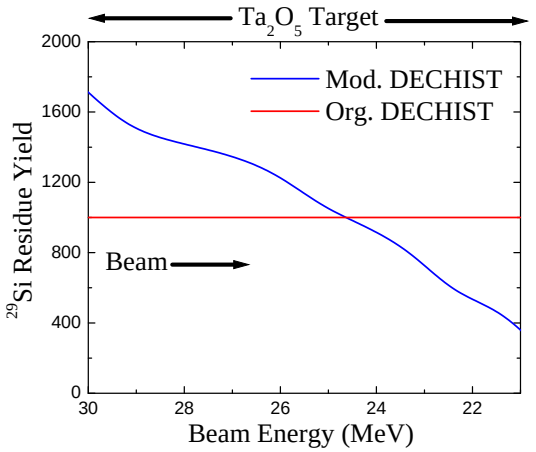

FIG. 3: (Color online) Cross-section of the residue as a function of beam energy. The original DECHIST program assigns uniform cross section (red line) of the residue while the modified DECHIST program incorporates beam energy dependent cross section (blue line) along the target thickness.

DECHIST program, that simulates the stopping of a given number of recoiling residues, divides the target thickness into bins equal to the (user) given number of recoil nuclei and treats each bin as the origin of one recoil nucleus. This is schematically represented in Fig. 3. As discussed above, this is a valid approximation for a thin target through which the beam energy can be assumed to remain unaltered and thus produce the residues with uniform probability (cross-section).

In the modified version of the DECHIST program used in the present work, changes have been implemented to incorporate the cross-section dependence of the residues on the changing beam energy along the thickness of the target. In the present version of DECHIST, upto 10 bins can be defined along the target thickness and relative cross-sections for the residue, in arbitrary units, can be specified therein, as illustrated in Fig. 3. The cross sections are preferably specified with reference to available experimental data or, in its absence, from statistical model calculations. It follows that the total thickness of the aforesaid bins is the thickness of the target that contributes in the production of the residues while the remaining thickness contributes only in the stopping process. It is to be stressed that the knowledge of the target thickness contributing to the residue production emerges from the consideration of the energy dependence of the relevant cross section and is imperative in the lifetime analysis in thick target setups.

It is understood that the aforesaid cross-section dependence on the changing beam energy would have a significant impact on the lifetime analysis of very short lived states, with $\tau \sim$ tens of fs, exhibiting completely shifted peaks in the angular ($\neq 90^o$) spectra. The reason can be perceived as the fast de-excitation following the short lifetime of the states occurs over a small fraction of the total stopping time and thus is sensitive to the number of residues produced with a given recoil energy, an estimation of which comes from the cross-section considerations. The reaction ^{18}O(^{16}O,$xnyp$), used in the present work, has also produced ^{29}Si as one of the residues, with several short lived levels (decaying with fast transitions) whose lifetimes have been previously reported. The Doppler shifts of the corresponding de-exciting γ-ray peaks have been analyzed to demonstrate the effect of inclusion of the cross-section dependence. For instance, let us consider the 5254 keV level in the ^{29}Si nucleus, de-exciting by 1631 keV transition. The reported lifetime of the level is 118±6 fs [12]. The corresponding peak appears shifted in the forward and the backward angles, as illustrated in Fig. 1. The lifetime analysis, following the procedure detailed subsequently in the paper, has been carried out in the 1596 keV (bottom) gate. Owing to the side-feeding(sf) contribution in the bottom gate, only the upper limit ($\tau_{level} + \tau_{sf}$) on the level lifetime could be obtained. The lifetime obtained without the inclusion of the cross-section effect is $\tau \leq 74$ fs, that is distinctly discrepant with respect to the reported value. The corresponding fit is illustrated in Fig. 4. As already indicated before, ignoring the cross-section dependence implied that the residue could be produced within the entire thickness of the target (9.25 mg/cm^2). However, the statistical model calculations indicate that the production of ^{29}Si occurs only upto a thickness of 4.4 mg/cm^2. The lifetime obtained using this thickness, with a uniform production cross-section throughout, is $\tau \leq 190$ fs. Further, if a cross-section dependent binning within the thickness of 4.4 mg/cm^2 is incorporated, the resulting lifetime is $\tau \leq 169$ fs, which is in better conformity with the reported value. Moreover in the latter case, the quality of lineshape fit is substantially better than the fit obtained in the analysis with full target thickness of 9.25 mg/cm^2, as illustrated in Fig. 4. This exercise demonstrates the importance of including cross-section effects in DSAM analysis for thick target experiments.

IV. DENSITY CONSIDERATIONS IN OXIDE TARGETS

Most of the molecular targets used in nuclear spectroscopy experiments come in the form of oxides. It is possible that these oxides appear in several structural phases of varying density. The problem is further compounded, if the targets are prepared through thermal oxidation which results in the formation of temperature dependent oxidation states. The preparation may also lead to the formation of non-crystalline (amorphous)

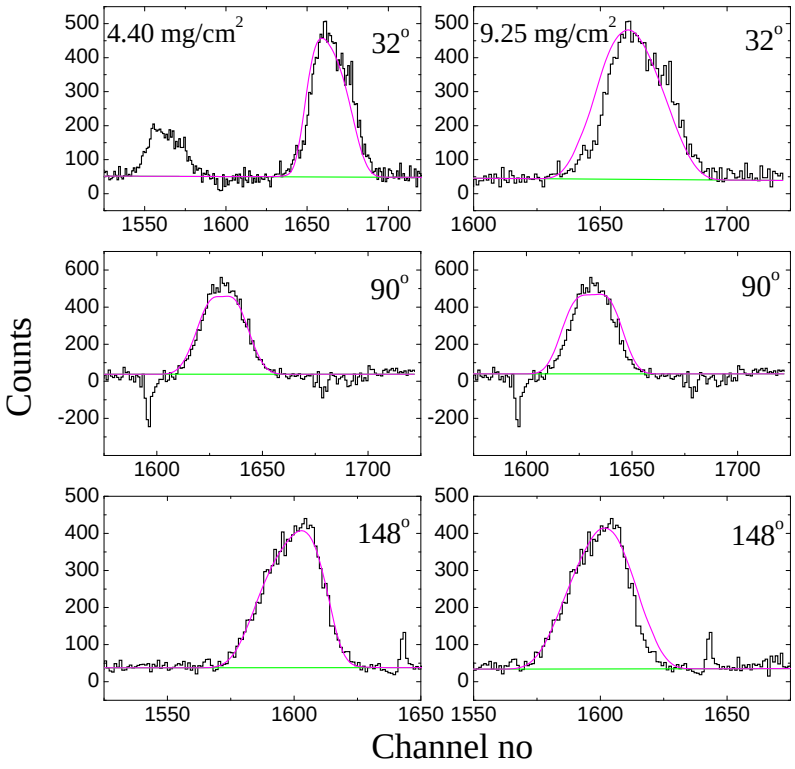

FIG. 4: (Color online) Least square fitting of the 1631 keV peak from the ^{29}Si nucleus, at 32°, 90° and 148°, using the LINESHAPE package. The peak exhibits Doppler shifts at the forward and the backward angle. The fits correspond to the target thickness 4.4 mg/cm^2 (effective) and 9.25 mg/cm^2 (total), respectively.

component. The consequent uncertainty pertaining to the structural composition of oxide targets can result in substantial discrepancies in the simulation of the stopping process and the lifetimes extracted therefrom. Thus, it is imperative to carry out a detailed investigation on the structural composition of the oxide target before concluding on the physical characteristics (density etc.) that sensitively affects the slowing / stopping mechanism of the recoils in the target medium.

One of the effective tools to investigate the structural composition of the target is X-Ray Diffraction (XRD). The XRD measurements have been carried out for the Ta_2O_5 target using Bruker D8 Advance x-ray diffractometer. A copper source provided x-ray of wavelength 1.5418 $\dot{A}$. The spectrum has been acquired in θ-2θ geometry with a step size of 0.02° in the range of 5° to 70°. The obtained diffraction pattern is presented in Fig. 5. The observed peaks have been assigned to both monoclinic and orthorhombic phases of crystalline Ta_2O_5. The inset of Fig. 5 shows a magnified view of the pattern in the range of 10 and 25°. The clear hump observed around 12° indicates presence of amorphous phase in the sample along with the crystalline phases.

The target has also been probed by Field Emission

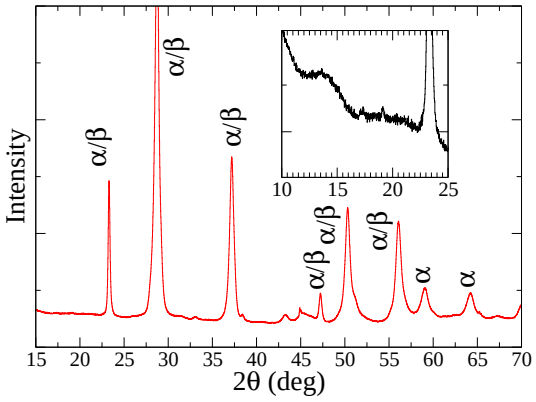

FIG. 5: (Color online) X-ray diffraction pattern obtained for Ta_2O_5 target. The intensity scale is linear. The monoclinic and the orthorhombic phases of crystalline Ta_2O_5 are identified by α and β labels, respectively. The inset depicts the pattern at low angles. The observed hump at the low angles may be attributed to the presence of amorphous phase (see text).

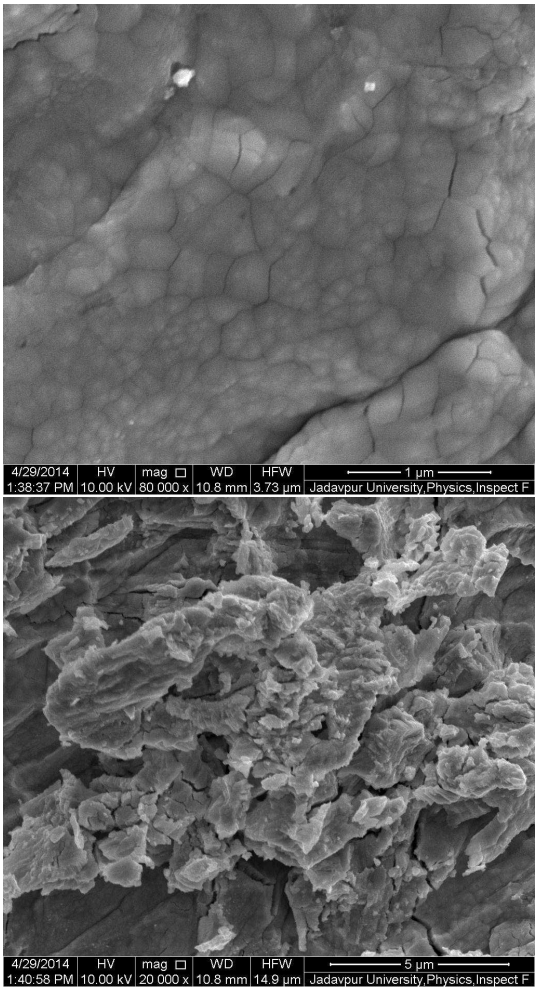

FIG. 6: Scanning Electron Micrograph images for Ta_2O_5 target. The upper panel illustrates the crystalline component while the bottom panel indicates the presence of amorphous component.

Scanning Electron Microscopy (FESEM) using an INSPECT F50 scanning electron micrograph. A few selected micrographs are illustrated in Fig. 6. The upper panel shows a selected area of the target that confirm polycrystalline nature of the target with clear view of grain boundaries. The lower panel of Fig. 6 depicts white fluffy parts of the target confirming presence of amorphous phase in the sample.

From the XRD and the SEM measurements it is thus concluded that the Ta_2O_5 consist of both crystalline and amorphous phases. However, the quantification of the respective components is not feasible in the present case. The manifestation of the presence of these multiple phases in oxide targets could be a modification in the density of the target medium, a critical parameter in the stopping calculations. The effect of composite phases and components renders an ambiguity in the choice of the density parameter. This could be addressed if

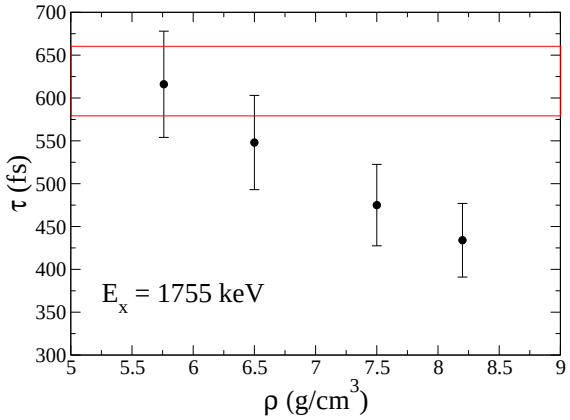

FIG. 7: (Color online) Variation of calculated lifetime for the 1755 keV state in the ^{32}P nucleus as a function of the density of the Ta_2O_5 target. The red band indicates the reported lifetime of the level along with the uncertainties.

one considers a variation in the density to reproduce previously measured lifetimes.

As mentioned earlier, the detailed investigation of the level lifetimes of ^{32}P by Kangasmäki *et al.* [8] justifies their use as calibration to determine the effective density of the Ta_2O_5 target medium. The calculated density of Ta_2O_5 from simple averaging of the elemental solid densities is 5.76 g/cm^3 while the maximum theoretical density is 8.2 g/cm^3. The latter is also recorded in the compound database of the SRIM package. The lifetime of the 1755 keV ($J_\pi = 3^+$) state in ^{32}P nucleus, de-exciting by the 1677 keV transition, has been obtained (following the procedure detailed in the subsequent section) as a function of the density and the corresponding plot is depicted in Fig. 7. As is evident from the figure, a density of 5.76 g/cm^3 produces the best compliance with the reported lifetime for the state. This value has also been used in the lifetime analysis for the other nuclei populated in the same experiment and the results are in agreement with the previously reported measurements. In the light of these results, this density has been used in all subsequent analysis reported in the present work.

It may be pointed out that for Ta_2O_5 in particular, it has been demonstrated by Martin *et al.* [19] that physical properties, such as density, are affected by the presence of microstructures originating from the fabrication methods which may justify the present empirical approach. Precedence for such method has recently been reported by Peters *et al.* [20] for oxide targets.

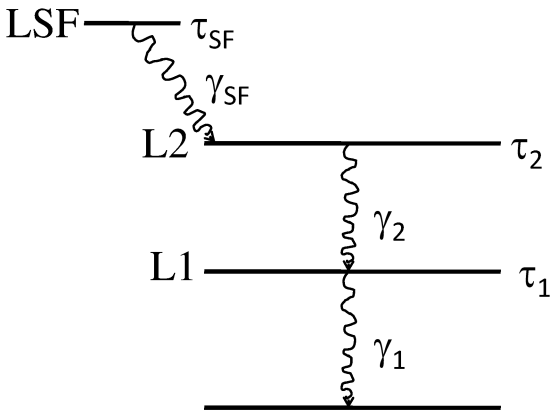

FIG. 8: Schematic representation of the Gating from Transition Above (GTA) procedure for determination of the level lifetime, as applied in the present work (see text).

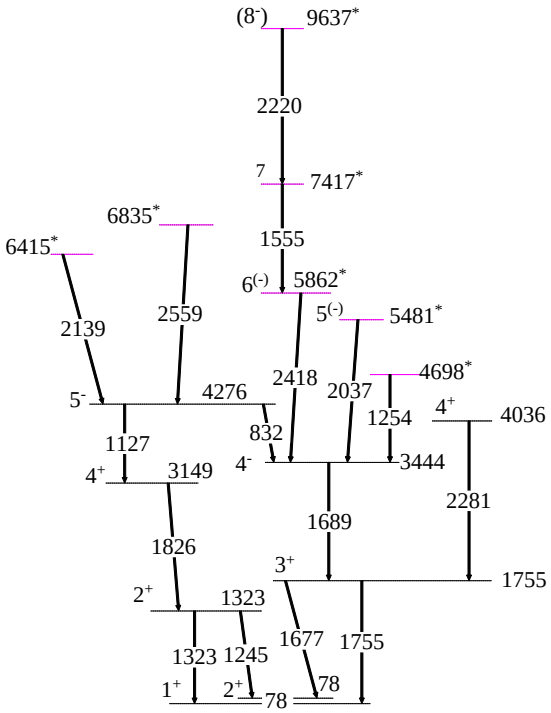

FIG. 9: (Color online) Partial level scheme of ^{32}P illustrating levels whose lifetimes have been measured in the present work. The lifetimes of the levels marked * have been measured for the first time in the present investigation.

V. DATA ANALYSIS AND RESULTS

This section describes the procedure adopted in the present DSAM analysis along with the various parameters used to obtain the level lifetimes of the ^{32}P nucleus. Monte Carlo simulation of the stopping process in the thick Ta_2O_5 target has been carried out with the modified DECHIST program for 10000 histories. Stopping powers used for the simulation have been obtained using the SRIM package. The cross-section for the production of the ^{32}P residue as a function of beam energy has been obtained from the statistical model calculations using the PACE4 code [21] and incorporated in the stopping calculations. A time step of 0.002 ps has been chosen for the simulation. The velocity profiles of the residual nuclei for detectors at 148^o, 123^o, 90^o, 57^o and 32^o have been individually calculated using the HISTAVER program.

The program LINESHAPE has been used to calculate the expected Doppler shape for a given γ-ray transition peak at a particular angle and perform least-square fit to the corresponding experimental spectrum in order to extract the level lifetime (τ). The γ-ray spectra at five different angles have been fitted simultaneously for determination of the lifetime. The spectra have been generated with gates on transition either above (GTA) or below (GTB) the transition of interest, in the level scheme. In case of the GTB procedure, the side-feeding is one of the crucial factors in the lifetime estimation and has been modelled in the present case with a single step feeder level. The lifetime of this feeder level is a variable parameter in the least-square fitting process. It is understood that in the GTB procedure, due to contributions from a dominant side-feeding process, one can only estimate an upper limit of the level lifetime which is the sum of the level lifetime and the side-feeding time, resulting from the least-square fitting exercise. In contrast, the GTA technique, which eliminates the side-feeding contribution, is a more deterministic analysis resulting into the actual lifetime of the level of interest. However, often owing to the sparse statistics in the peak of interest, particularly in the high spin states populated in the heavy-ion induced fusion-evaporation reaction, the GTA may have a limited scope in the lifetime analysis of the acquired data. The application of the GTA procedure in the present work is schematically represented in Fig. 8 . Let us assume that L1 is the level of interest, de-excited by the γ_1 transition. In the GTA technique, the L1 level lifetime has to be extracted from the γ_2 gate (de-exciting level L2). LSF is the side-feeder to L2. In the first step, the lifetime (τ_2) and the side-feeding time (τ_{SF}) of L2 are extracted from the lineshape analysis of the γ_2 transition from the γ_1 gated spectra. The lifetime of L2 (τ_2) and the corresponding side-feeding time (τ_{SF}) can be perceived as the feeding (formation) time distribution of the level L1. In the second step of the analysis, the lifetime of L1 is determined from the lineshape analysis of the γ_1 peak in the γ_2 gated spectra, wherein the τ_2 and

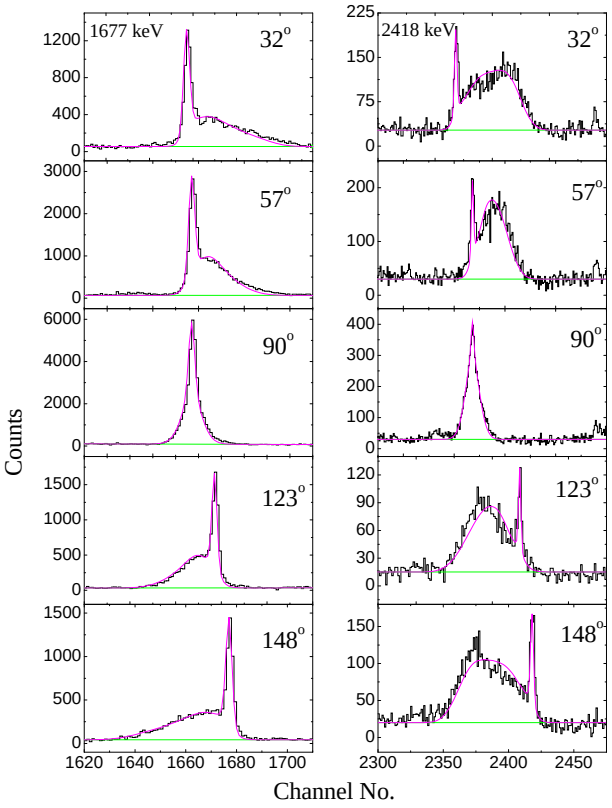

FIG. 10: (Color online) Representative fits of the Doppler shapes of the 1677 keV and the 2418 keV transitions from the ^{32}P nucleus, obtained in the present work.

the τ_{SF}, representing the feeding time distribution of L1, are provided as inputs and held fixed in the least-square fitting process. The least-square fitting parameters include those pertaining to the experimental spectrum such as the background, peak height and the contaminant peaks. These parameters are initially varied in the minimization procedure but eventually held fixed, corresponding to the best fit, while determining the final value of the level lifetime. Chi-square analysis has been carried out to estimate the uncertainties on the level lifetimes. However, the principal uncertainty in the lifetime measurements originate from the errors pertaining to the estimation of the stopping powers used in the calculations. Typically, these uncertainties are known to be $\sim$ 10%. Thus, the stopping powers have been varied by $\pm$10% and the resulting dispersion in the level lifetimes have been included in the quoted uncertainties.

The lifetimes of the states in the ^{32}P nucleus, derived from the present work, are summarized in Table I and the partial level scheme of the nucleus, illustrating the aforesaid levels, is depicted in Fig. 9. Representative fits to the observed lineshape are illustrated in Fig. 10. As included in Table I, lifetimes, or upper limits on

TABLE I: Lifetimes of the states in ^{32}P from the present work in comparison to the previously reported values. The quoted uncertainties include the effect of the uncertainties in the stopping powers. Please refer to the text for details.

J_i^π	E_x (keV)	E_γ (keV)	τ (fs) Present Work	NNDC
2_2^+	1323	1323	485^{+57}_{-32}	488^{+25}_{-25}
		1245	472^{+38}_{-23}	
3_1^+	1755	1677	616^{+65}_{-46}	620^{+40}_{-40}
4_1^+	3149	1826	$< 745^{+83\,a}_{-76}$	498^{+36}_{-36}
4_1^-	3444	1689	$< 883^{+103\,a}_{-82}$	387^{+45}_{-45}
4_2^+	4036	2281	$< 80^{+22\,a}_{-10}$	35^{+25}_{-25}
5_1^-	4276	1127	$< 696^{+99\,a}_{-42}$	779^{+115}_{-115}
		832	$< 902^{+85\,a}_{-101}$	
	4698	1254	$< 579^{+69\,a}_{-62}$	
$5_2^{(-)}$	5481[b]	2037	$< 188^{+36\,a}_{-29}$	
$6_1^{(-)}$	5862[b]	2418	$< 629^{+82\,a}_{-61}$	
	6415[b]	2139	$< 186^{+30\,a}_{-30}$	
	6835[b]	2559	$< 159^{+30\,a}_{-23}$	
$7^{(-)}$	7417[b]	1555	$< 1018^{+130\,a}_{-82}$	
(8^-)	9637[b]	2220	$< 220^{+30\,a}_{-27}$	

[a]The presence of a dominant side-feeding allowed for assignment of only an upper limit on the lifetime.

[b]New level, first reported in our earlier work [5]

the same, of 13 levels have been extracted from the present study. Of these, lifetimes for 6 states (1323, 1755, 3149, 3444, 4036 and 4276 keV) were previously known while an upper limit on that of the remaining 7 states have been reported for the first time following the present investigation. Owing to the sparse statistics in the gated spectra, lifetimes of only a few levels could be determined by the GTA technique while for the other levels, the GTB procedure has been carried out. Consequently, only an upper limit on the corresponding level lifetime could be assigned.

The GTA technique could be carried out to determine the lifetimes of the levels at 1323 keV and 1755 keV. For the 1323 keV transition, the feeding time distribution, as defined earlier, has been determined by analyzing the lineshape of the 1826 keV transition in the 1323 keV gated spectra. This feeding time distribution has been

kept fixed to determine the lifetime of the 1323 keV level, through least square fitting of the Doppler shape of the 1323 keV peak, in the 1826 keV gated spectra. The lifetime of the 1323 keV level has also been determined from the Doppler shape analysis of the 1245 keV peak, observed in the 1826 keV gate. The lifetime of the level resulting from the analysis of the two individual transitions are in excellent agreement, as recorded in Table I, and is in compliance with the previously reported lifetime for the level. As far as the lifetime analysis of the 1755 keV level is concerned, feeding time distribution has been extracted from the analysis of the lineshape of the 1689 keV transition observed in the 1677 keV gated spectra. This distribution has been used in the lifetime analysis of the 1755 keV level in the 1689 keV gated spectra. The lifetime (616 fs) obtained therefrom is in excellent overlap with the previously reported value (620 fs). This exercise demonstrates the feasibility of undertaking DSAM analysis on data acquired from thick molecular targets.

Upper limits on the lifetimes of the remaining levels have been obtained from the GTB procedure and included in Table I.

The experimental level lifetimes, obtained from the present analysis, are compared with those from large basis shell model calculations, as detailed in the next section.

VI. SHELL MODEL CALCULATIONS

Nuclei at the interface of *sd*-fp shells have been extensively probed within the framework of large basis shell model calculations [2, 7]. Lifetime measurements provide stringent testing grounds for these theoretical calculations, in particular for the validation of the two-body interactions. In recent times there have been developments of new interactions for these nuclei, that incorporates the contemporary experimental findings [2, 7, 22]. In the present work, large basis shell model calculations for the ^{32}P nucleus have been carried out. Lifetime results obtained from the present experiment as well as from the previous studies have been compared with the model predictions. The shell model code NuShellX@MSU [23] has been used for the purpose, wherein different model spaces and interactions have been used for a comprehensive comparison.

The positive parity states have been calculated using the *sd* model space, consisting of the $1d_{5/2}, 2s_{1/2}, 1d_{3/2}$ orbitals, and with the $USDA$ interaction. The effective nucleon charges used are $e_p = 1.36$ and $e_n = 0.45$ [2]. The results are summarized in Table II. The calculated lifetime of the 1323, 1755, 3149 keV states, are in excellent agreement with the measurements.

The negative parity states essentially originate from the $1p-1h$ excitations into the fp shell. These have been calculated using the $sdpf$ model space, consisting of the $1d_{5/2}, 2s_{1/2}, 1d_{3/2}$, $1f_{7/2}, 2p_{3/2}, 2p_{1/2}, 1f_{5/2}$ orbitals, along with the $sdpfmw$ and the $sdpfmu$ interactions. The effective nucleon charges used are, identical to the $USDA$ interaction, $e_p = 1.36$ and $e_n = 0.45$. A truncation scheme has been implemented, allowing maximum one neutron particle in the fp shell, either in the $1f_{7/2}$ or in the $2p_{3/2}$ orbital. This was necessiated owing to the fact that the calculations with the full fp shell resulted in considerable lowering of the predicted excitation energies. The results (level energies and lifetimes) of the model calculations in comparison to the experimental findings are recorded in Table II. The experimental transition probabilities (B(M1), B(E2)) and the branching ratios are compared with the shell model predictions in Table III. Results for the 3^- and 4^- states, that decay by E1 transitions, could not be compared with the shell model calculations. The calculations are in general agreement with the experimental results. The deviations between the experimental and the calculated quantities, particularly for the negative parity states, may warrant re-evaluation of the two-body matrix elements in this region.

VII. CONCLUSION

Lifetime of the excited states in the ^{32}P nucleus have been measured using the DSAM technique, carried out with thick molecular targets. The extended analysis procedure has been validated with respect to the previously reported measurements. Upper limit on lifetimes of the levels, E_x = 4698, 5481, 5862, 6415, 6835, 7417 and, 9637 keV, in the nucleus have been determined for the first time. Experimental results have been compared with the shell model calculations for states for which the spin-parity assignments were known from earlier studies. The positive parity states have been successfully interpreted using the $USDA$ interaction. The cross shell calculations using the $sdpfmw$ and the $sdpfmu$ interactions for the negative parity states exhibit comparable results, which are in satisfactory agreement with the experimental observations. The presence of transitions with $\tau \sim 200$ fs around $E_x \sim 6$ MeV may indicate the possible onset of collectivity and warrants the necessity of further investigation. This work demonstrates the feasibility of undertaking DSA measurements using a molecular target, thus extending the scope of the technique. However, understanding of the structural composition and the stopping characteristics of the target medium have been identified to remain as the essential inputs in such endeavours.

TABLE II: Comparison of experimental and shell model calculated level energies and lifetimes in ^{32}P. The states with lifetimes measured in the present work have been marked in bold font.

E_x	J^π	τ		Shell Model Calculation					
				USDA		SDPFMW		SDPFMU	
		This Work	NNDC	E_x	τ	E_x	τ	E_x	τ
(keV)		(fs)	(fs)	(keV)	(fs)	(keV)	(fs)	(keV)	(fs)
0	1_1^+			0	0	6		0	
78	2_1^+		-	177	60280	0		4	
513	0_1^+		2641 ± 115	646	4355	260	17988	216	39221
1149	1_2^+		264 ± 17	1030	616	1048	154	1109	102
1323	2_2^+	$\mathbf{485^{+57}_{-32}}$	**488 ± 25**	**1291**	**487**	**1135**	**2941**	**1162**	**2181**
1755	3_1^+	$\mathbf{616^{+65}_{-46}}$	**620 ± 40**	**1832**	**729**	**1528**	**1215**	**1595**	**854**
2177	3_2^+		76 ± 14	2292	36	2225	54	2309	49
2218	2_3^+		240 ± 25	2314	124	2037	101	2175	46
2658	2_4^+		12 ± 4	2594	10.5	2602	10	2570	10
3149	4_1^+	$< \mathbf{745^{+83}_{-76}}$	**498 ± 36**	**3219**	**370**	**3168**	**124**	**3132**	**131**
4036	4_2^+	$< \mathbf{80^{+22}_{-10}}$	**35 ± 25**	**4119**	**10.3**	**3727**	**12**	**3857**	**10**
4276	5_1^-	$< \mathbf{902^{+85}_{-101}}$	**779 ± 115**			**4106**	**927**	**3576**	**1257**
5481	$5_2^{(-)}$	$< \mathbf{188^{+36}_{-29}}$				**5358**		**4886**	
5862	$6_1^{(-)}$	$< \mathbf{629^{+82}_{-61}}$				**5640**	**190**	**5136**	**250**
7417	$7_1^{(-)}$	$< \mathbf{1018^{+130}_{-82}}$				**6846**	**80**	**6189**	**108**
9637	(8_1^-)	$< \mathbf{220^{+30}_{-27}}$				**8834**	**127**	**8009**	**213**

ACKNOWLEDGMENT

The authors thank all the participants of the INGA collaboration for their help in setting up the facility at IUAC, New Delhi. We are thankful to J. P. Greene (ANL, USA) for the ^{18}O target. We thank the Pelletron staff at IUAC, New Delhi for their excellent support during the experiment. Discussions with Prof. Alex Brown on the shell model calculations have been of much help and are deeply appreciated. The help in SEM measurements received from Dr. S. Kumar and Dr. S. Das of the Department of Physics, Jadavpur University is gratefully acknowledged. The SEM facility at the Department of Physics, Jadavpur University is supported by the Department of Science and Technology (DST), Government of India, under the FIST Program. SSB would like to acknowledge the financial assistance in the form of a fellowship (SRF, CSIR sanction No. 09/838(0038)2010-EMR-I) from the Council of Scientific and Industrial Research (CSIR), Government of India. The INGA Project is partially supported by the DST under Grant No. IR/S2/PF-03/2003-III.

TABLE III: Comparison of the experimental transition probabilities and branching ratios, wherever possible, with those from the shell model calculations. The assignments (M) are quoted from NNDC [12] and/or previous work [5].

			Experimental			Shell Model								
E_x	E_γ	M				USDA			SDPFMW			SDPFMU		
(keV)	(keV)		B(M1) (μ_n^2)	B(E2) (e^2fm^4)	BR	B(M1) (μ_n^2)	B(E2) (e^2fm^4)	BR	B(M1) (μ_n^2)	B(E2) (e^2fm^4)	BR	B(M1) (μ_n^2)	B(E2) (e^2fm^4)	BR
1323	1323	M1	$0.027^{+0.002}_{-0.003}$	-	0.53±0.01	0.041	-	0.68	0.007	-	0.71	0.008	-	0.63
	1245	M1	$0.029^{+0.002}_{-0.003}$	-	0.47±0.01	0.031	-	0.32	0.002	-	0.25	0.004	-	0.31
1755	1755	E2+M3	-	$0.796^{+0.076}_{-0.064}$	0.010±0.001	-	0.782	0.02	-	0.033	0.00	-	0.398	0.00
	1677	M1+E2	$0.012^{+0.001}_{-0.001}$	$37.611^{+3.035}_{-3.590}$	0.98±0.02	0.001	50.490	0.86	0.003	56.010	0.94	0.006	66.160	0.96
	432	M1+E2	$0.022^{+0.002}_{-0.002}$	$24.980^{+2.033}_{-2.370}$	0.020±0.001	0.027	0.327	0.11	0.043	0.395	0.05	0.032	0.348	0.03
3149	3071	E2+M3	-	$0.299^{+0.024}_{-0.020}$	0.050±0.004	-	0.571	0.07	-	3.164	0.15	-	5.096	0.22
	1826	E2+M3	-	$44.980^{+3.032}_{-3.505}$	0.56±0.02	-	50.460	0.73	-	34.97	0.18	-	44.980	0.20
	1394	M1+E2	0.000	$41.766^{+3.255}_{-2.816}$	0.14±0.01	0.002	46.880	0.14	0.056	50.74	0.63	0.061	60.840	0.54
	972	M1+E2	$0.031^{+0.002}_{-0.002}$	$5.645^{+0.439}_{-0.381}$	0.25±0.01	0.011	5.370	0.06	0.018	4.79	0.03	0.030	2.343	0.04
4036	2281	M1+(E2)	$0.137^{+0.342}_{-0.069}$	-	1.00	0.267	9.583	0.59	0.303	3.609	0.68	0.328	3.270	0.63
4276	832	M1+E2	$0.096^{+0.016}_{-0.013}$	$38.890^{+6.737}_{-5.001}$	0.77±0.12	-	-	-	0.076	8.783	0.95	0.094	11.380	0.99
5862	1586	(M1)	> 0.001	-	0.030±0.002	-	-	-	0.004	-	0.05	0.011	-	0.18
	2418	E2+M3	-	> 13.986	0.89±0.02	-	-	-	-	46.700	0.95	-	37.770	0.81

[1] B. A. Brown and B. H. Wildenthal, Annu. Rev. Nucl. Part. Sci. **38**, 29 (1988).

[2] W. A. Richter, S. Mkhlze, and B. A. Brown, Phys. Rev. C **78**, 064302 (2008).

[3] R. Chakrabarti, S. Mukhopadhyay, Krishichayan, A. Chakraborty, A. Ghosh, S. Ray, S. S. Ghugre, A. K. Sinha, L. Chaturvedi, A. Y. Deo, et al., Phys. Rev. C **80**, 034326 (2009).

[4] P. C. Bender, C. R. Hoffman, M. Wiedeking, J. M. Allmond, L. A. Bernstein, J. T. Burke, D. L. Bleuel, R. M. Clark, P. Fallon, B. L. Goldblum, et al., Phys. Rev. C **80**, 014302 (2009).

[5] R. Chakrabarti, S. Mukhopadhyay, R. Bhattacharjee, S. S. Ghugre, A. K. Sinha, A. Dhal, L. Chaturvedi, M. K. Raju, N. Madhavan, R. P. Singh, et al., Phys. Rev. C **84**, 054325 (2011).

[6] S. S. Bhattacharjee, R. Bhattacharjee, R. Chakrabarti, R. Raut, S. S. Ghugre, A. K. Sinha, T. Trivedi, L. Chaturvedi, S. Saha, J. Sethi, et al., Phys. Rev. C **89**, 024324 (2014).

[7] W. A. Richter and B. A. Brown, Phys. Rev. C **80**, 034301 (2009).

[8] A. Kangasmäki, P. Tikkanen, J. Keinonen, W. E. Ormand, and S. Raman, Phys. Rev. C **55**, 1697 (1997).

[9] P. E. Carr, D. C. Bailey, L. L. Green, A. N. James, J. F. Sharpey-Schafer, and D. A. Viggars, J. Phys. A **6**, 705 (1973).

[10] F. E. H. van Eijkern, G. V. Middelkoop, J. Timmer, and J. A. van Luijk, Nucl. Phy. A **210**, 38 (1973).

[11] J. C. Wells and N. R. Johnson, ORNL Report **6689**, 44 (1991).

[12] URL `www.nndc.bnl.gov`.

[13] S. Muralithar, K. Rani, R. Kumar, R. P. Singh, J. J. Das, J. Gehlot, K. S. Golda, A. Jhingan, N. Madhavan, S. Nath, et al., Nucl. Instr. Meth. Phys. Res. A **622**, 281 (2010).

[14] D. Ward, AECL **5313** (1976).

[15] J. F. Ziegler, *The Stopping and Ranges of Ions in Matter* (Pergamon Press, 1980).

[16] L. C. Northcliffe and R. F. Schilling, At. Data Nucl. Data Tables **7** (1970).

[17] URL `www.srim.org`.

[18] J. B. Snyder, Ph.D. thesis, Washington University (2013).

[19] P. J. Martin, A. Bendavid, M. Swain, R. P. Netterfield, T. J. Kinder, W. G. Sainty, D. Drage, and L. Wielunski, Thin Solid Films **239**, 181 (1994).

[20] E. E. Peters, A. Chakraborty, B. P. Crider, B. H. Davis, M. K. Gnanamani, M. T. McEllistrem, F. M. Prados-Estàvez, J. R. Vanhoy, and S. W. Yates, Phys. Rev. C **88**, 024317 (2013).

[21] A. Gavron, Phys. Rev. C **21**, 230 (1980).

[22] F. Nowacki and A. Poves, Phys. Rev. C **79**, 014310 (2009).

[23] B. A. Brown and W. D. M. Rae, MSU-NSCL Report (2007).